High-order direct and large eddy simulations of turbulent flows in rotating cavities

Serre E.

1 Introduction

The simulation of rotating cavities flows is a major issue in computational fluid dynamics and engineering applications such as disk drives used for digital disk storage in computers, automotive disk brakes, and especially in turbomachinery (see a review in [8]).

Centrifugal and Coriolis forces produce a secondary flow in the meridian plane composed of two thin boundary-layers along the disks separated by a non-viscous geostrophic core where the axial gradient of pressure nearly equilibrates the Coriolis force. That produces adjacent coupled flow regions that are radically different in terms of the flow properties and the thickness scales involving very challenging simulations. Very thin non-parallel boundary layers governing the flow stability develop along the stationary and the rotating disks, called thereinafter Bödewadt and Ekman layer, respectively.

As a consequence, besides its primary concern to industrial applications, the rotating disks problem has also proved a fruitful means of investigating transition to turbulence and the effects of mean flow three-dimensionality on the turbulence and its structure [6, 11]. Indeed, these boundary layers are three-dimensional from their inception and constitute one of the few non-trivial three-dimensional cases whose Navier-Stokes solutions exist.

Linear stability analysis has revealed that such boundary layer is subject to two generic types of instability. An inviscid instability, due to the inflectional nature of the velocity profile, is labeled type I, whereas type II is due to the combined action of viscous and Coriolis effects (see the review by [2]). The matter of the transition scenario is currently much debated around the idea that a global instability might take place and lead to transition to turbulence. A new light on the problem was given by Lingwood's discovery [5] that such boundary layer underwent transition

Serre, M2P2 UMR 6181, CNRS - Universite Aix-Marseille, France, e-mail: Eric.Serre@L3m.univ-mrs.fr

H. Kuerten et al. (eds.), *Direct and Large-Eddy Simulation VIII*,
ERCOFTAC Series 15, DOI 10.1007/978-94-007-2482-2_64,

from convective to absolute behavior at a local Reynolds number (dimensionless radius, r/δ, $\delta = (\nu/\Omega)^{1/2}$)) (507) close to the onset of turbulence (513). But to this day, if further studies have confirmed these local linear stability results, no general agreement exists concerning their outcome in terms of global behavior. Pier's theoretical work [9], showing the possible existence of a global nonlinear elephant mode, together with Davies and Carpenter's numerical results [3], demonstrating linear global stability, would imply a subcritical global bifurcation, which has been demonstrated in [14]. This behavior would then be the outcome of the competition between the stabilizing non-parallel effects, and the destabilizing nonlinear ones, so that both have to be taken into account. This is done here, where DNS is used to investigate the impulse response of the boundary layer encountered in a rotating disk configuration with radial throughflow.

Simulation of turbulent rotating cavities flows remains a challenge. Due to the skewing of the boundary layers [11], Reynolds stresses are not aligned with the mean flow vector that invalidates eddy-viscosity models. Besides, such models clearly fail to predict turbulent flow by delaying the transition along the rotor. Second moment closures provide a more appropriate level of modeling, but the Reynolds stress behavior is not fully satisfactory, particularly near the rotating disk (see a review in Launder *et al.* [4]). Moreover, the existence of persisting large-scale 3D precessing vortices at high Reynolds numbers requires strongly unsteady computations. As a consequence, LES seems to be right level of modeling. Nevertheless, the literature on the topic is rare. Wu and Squires [15] performed the first LES of the flow over a single rotating disk using dynamic and mixed dynamic Smagorinsky models to analyze the mechanisms promoting sweeps and injections. First computations treating the rotor-stator flow as unsteady were DNS of Lygren and Andersson [7] and Serre *et al.* [10]. Finally, Anderson and Lygren [1] carried out the first LES in a sector with periodic boundary conditions to reduce the costs. The use of spectrally accurate numerical schemes adds a difficulty due to the fact that spectral approximations are much less diffusive than low order ones, involving an accumulation of the energy on the high spatial frequencies which finally leads to the divergence of the computations. This is for all these reasons that we proposed in our group an original approach based on the spectral vanishing viscosity (SVV), first introduced by Tadmor [13] to stabilize resolution of hyperbolic equation. This alternative LES formulation is proposed and incorporated into the Navier-Stokes equations for controlling high-wavenumber oscillations [12]. Flow predictions at $Re = 10^6$ are provided in a closed rotor-stator cavity in order to avoid difficulties related to in-outflow conditions.

2 Modeling

We consider the flows within rotating cavities composed of two disks enclosing an annular domain of radii a and b with $b > a$. The domain can be open (rotating

cavity) with a forced radial flow imposed at $r = a$ or eventually bounded by two coaxial cylinders of height $2h$ (rotor-stator cavity). The geometry is characterized by an aspect ratio $L = (b-a)/2h$ and a curvature parameter $R_m = (b+a)/(b-a)$. For the rotating cavity ($L = 10$, $R_m = 5$), both disks rotate at uniform angular velocity $\Omega = \Omega e_z$, e_z being the unit vector on the axis while in the rotor-stator cavity ($L = 5$, $R_m = 1.8$) one disk is at rest. These configurations are basic cavity elements of a turbine engine.

The incompressible fluid motion is governed by the three-dimensional Navier-Stokes equations in primitive variables. The equations are made dimensionless by considering h, Ω^{-1} and Ωb as length, time and velocity of reference. No-slip boundary conditions are applied at all walls so that all the near-wall regions were explicitly computed. At the inflow of the rotating cavity velocity profiles are prescribed while at the outflow a convective boundary condition is applied.

The temporal discretization adopted in this work is a projection scheme, based on backwards differencing in time (see the details in [12]).

The solutions are searched as truncated series of Chebyshev polynomials of degree at most equal to N_r and N_z in the non-homogeneous radial and axial directions (r,z) respectively and Fourier series in the 2π-periodic tangential direction of cut off frequency $N_\theta/2$. To perform LES, a well controlled diffusion has been incor-

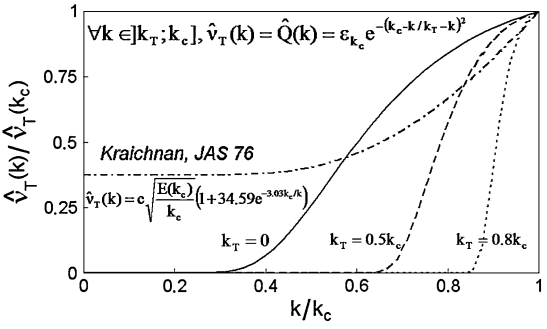

Fig. 1 Plot of the viscosity kernel $\hat{Q}$ together with the spectral eddy-viscosity of Kraichnan-Lesieur. $\hat{Q}$ is normalized by its maximum value at $\omega_N = \mathrm{N}\ (= 42)$ for two typical values of the threshold frequency $\omega_T = 0$ and $\omega_T = \sqrt{N}$

porated in the Navier-Stokes equations. A new diffusion operator Δ_{SVV} is simply implemented by combining the classical diffusion and the new SVV terms to obtain:

$$\nu\Delta_{SVV} \equiv \nu\Delta + \nabla.(\varepsilon_N Q_N \nabla) = \nu\nabla.S_N\nabla \tag{1}$$

where ν is the diffusive coefficient and where:

$$S_N = diag\left\{S^i_{N_i}\right\},\ S^i_{N_i} = 1 + \frac{\varepsilon^i_{N_i}}{\nu} Q^i_{N_i} \tag{2}$$

with $\varepsilon^i_{N_i}$ the maximum of viscosity and $Q^i_{N_i}$ a 1D viscosity operator acting in direction i, and defined in the spectral space by an exponential function: $\widehat{Q}^i_{N_i}(\omega) = 0$, if $0 \le \omega \le \omega^i_T$ and $\widehat{Q}^i_{N_i}(\omega) = \exp(-(\omega-\omega^i_T)^2/(\omega-\omega^i_T)^2)$ if $\omega^i_T \le \omega \le \omega^i_N$,

where ω_T^i is the threshold after which the viscosity is applied and ω_N^i the highest frequency calculated in the direction i. An illustration of the viscosity kernel in the spectral space together with the classical spectral eddy-viscosity kernel of Kraichnan-Lesieur is presented in Figure 1. Such model is only active for the short length scales and it has been shown that it keeps the spectral convergence (details in [12]). It is noticeable that the SVV term is not scaled with Re that implied that for a fixed grid and given SVV parameters, the SVV term may become larger relatively to the classical diffusion term when increasing Reynolds number.

3 Results

3.1 Transition to turbulence

The breakdown to turbulence in a rotating disk boundary-layer is analyzed via direct numerical simulation (DNS) in a sector ($2\pi/4$ or $2\pi/8$ depending the mesh resolution) of an annular cavity with a forced inflow at the hub and free outflow at the rim. The largest size of the mesh in the 1/4 cavity is $649 \times 170 \times 65$ in radial, azimuthal and axial directions that corresponds to a grid resolution of approximately ten and six Kolmogorov length scales in the radial and axial directions, respectively. Our objective here was to obtain a scenario of transition based on a cascade of absolute instabilities as conjectured in Pier [9] from model equations.

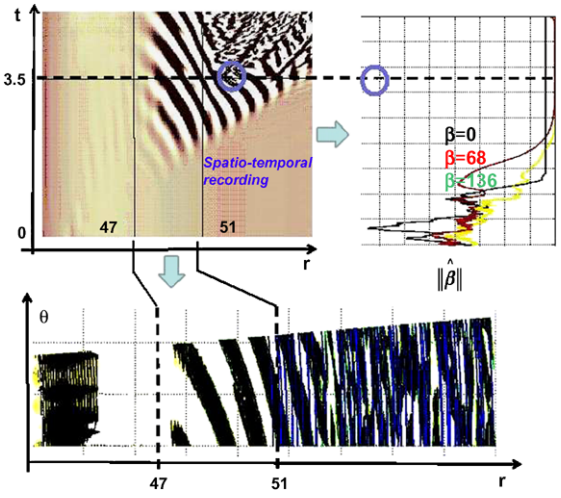

Fig. 2 Transition to turbulence in the rotating disk boundary layer showing a cascade of two global modes at $Re = 7 \times 10^5$. Spatio-temporal diagram (top-left), temporal evolution of the energy of the three main Fourier modes (top-right) and iso-surface of vertical component velocity (bottom). DNS results with $N_r = 649$, $N_z = 65$ and $N_\theta = 170$.

The global Reynolds number has been set to $Re = 7.10^5$, and the mass flow rate to $C_w (= Q/\nu b) = 1995$ which places the transition from convective to absolute instability in the first half of the cavity. Axisymmetric stationary base flow has been

reached by damping convective axisymmetric modes of instability (see details in [14]), generated by the inflow condition at each time-step. The nonlinear dynamics of the flow has been analyzed by superimposing an initial spatially localized perturbation during a single time step at the beginning of the computations. The perturbation velocity field corresponds to a Stokes flow over a hemispherical roughness located at the wall near the hub with an amplitude of 0.1% of the velocity maxima. Figure 2 presents the nonlinear evolution of such an initial perturbation with a 68-fold symmetry. The spatio-temporal diagram (Figure 2 (top-left)) shows only the saturated front of the wave packet. Shortly after the saturation of the first global instability, characterized by a trailing edge moving upstream and rapidly stabilizing close to $r = 47$, the saturated wave downstream of the trailing front starts being perturbed with order-unity close to $r = 51$ at $t = 3.5$. Behind that secondary front the state is disordered in time and space indicating incipient turbulence. Calculations eventually blow up at about $t = 10$ due to aliasing. Indeed, the resolution of the mesh being approximately ten and six Kolmogorov length scales in the radial and axial directions respectively, the turbulent dissipation scale is not resolved. Nevertheless, SVV computations can be run as long as wanted and confirm the limited in time DNS results. The associated spatial structure is shown by a horizontal cut on Figure 2 (bottom) showing the clockwise spiral (rotating counterclockwise in time) that saturates after the primary front at $r = 47$, developing secondary instability shortly before $r = 51$. At this secondary front, base flow modifications become of order unity (Figure 2 (top-right)). Close to this secondary front the harmonic component $m = 136$ also become of the same amplitude compared to the primary rolls, and higher harmonics start having a physically relevant amplitude. Finally, the associated turbulent kinetic energy in a vertical cut in Figure 3 confirms that non zero values occur just downstream the radial location of the secondary front at $r = 51$.

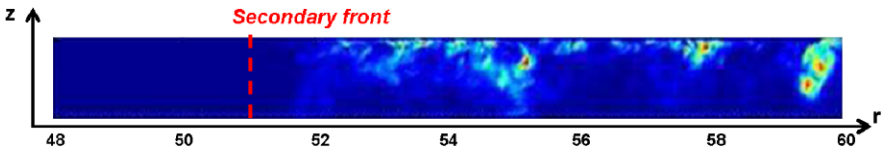

Fig. 3 Turbulent kinetic energy in the meridian plane showing the breakdown to turbulence downstream the primary front. Only the upper half-cavity is shown.

This scenario relies on low incoming noise upstream of the primary front, and a sufficiently strong impulsive perturbation as the first global bifurcation is known to be subcritical. For the first time it confirms the possibility of a direct transition to turbulence through an elephant cascade.

3.2 Turbulence

A detailed picture of the turbulent flow structure is provided by high-order LES in a closed rotor-stator cavity at Reynolds numbers $Re = 10^6$. The largest size of the mesh in the 1/2 cavity is $151 \times 240 \times 81$ in radial, azimuthal and axial directions that corresponds to a wall coordinate $z^+ \approx 1$ in both layers. SVV parameters have been set to $\varepsilon_N = (1/N, 1/N, 1/N)$ and $\omega_T = (2\sqrt{N}, 5\sqrt{N}, 4\sqrt{N})$ in (r, θ, z) directions respectively. The results published in [11] show that the mean flow is still composed of two boundary layers along the rotor and the stator separated by a geostrophic core like in the laminar regime. The agreement with LDV measurements is very satisfactory for the first and the second-order order statistics as well. The entrainment coefficient, $K = v/\Omega r$ at mid-radius, is equal to 0.38 compared to the experimental value $K = 0.42$. The prediction of this coefficient which is directly related to the pressure gradient (Taylor-Proudman theorem) is crucial to the design of thrust bearings. It emerges at this Reynolds number that the turbulence is mainly confined in the wall boundary layers including the layers along both cylinders closing the cavity, Figure 4. The stator boundary layer is fully turbulent. On the other hand, the rotor layer becomes progressively turbulent from the outer radial locations although the rotating hub is shown to destabilize the inner part of the boundary layers. The max of k is located at the jet impingement of the flow coming from the rotor. The turbulent flow is associated to quasi-axisymmetric coherent structures along the stator while in the transitional rotor-layer three-dimensional spiral arms can be still observed.

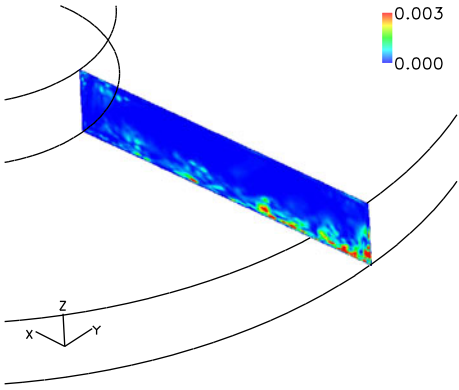

Fig. 4 Isolines map of the turbulent kinetic energy at $Re = 10^6$. LES-SVV results for a grid $N_r = 151$, $N_z = 81$, $N_\theta = 240$ and $\delta t = 10^-5$.

We have investigated the structural properties of the boundary layers along the disks. In particular, the structural parameter a_1 (the ratio of the magnitude of the shear stress vector to twice the turbulence kinetic energy) as well as the mean velocity angle ($\gamma_m = arctan(V_r/V_\theta)$) have been calculated. The truthfulness of the alignment assumption between the shear stress vector and the mean velocity gradient vector made in subgrid scale models using an eddy viscosity has also been checked. The mean velocity gradient angle ($\gamma_g = arctan((\partial_r V_r/\partial z)/(\partial_r V_\theta/\partial z))$) as

well as the turbulence shear stress angle ($\gamma_\tau = arctan((\overline{V_r' V_z'}/\overline{V_\theta' V_z'})$) along the radius of both disks have been evaluated. Results are summarized in the Table 1:

	γ_m (deg)	$\gamma_\tau - \gamma_g$ (deg)	max(a_1)
rotor	-0.5 / 16.5	0 / 94	0.058
stator	-34 / 0	0 / 151	0.062

Table 1 Structural properties of the boundary layers along the rotor and the stator. Mean velocity angle γ_m, mean velocity gradient angle γ_g and turbulence shear stress angle γ_τ as a function of the radius. a_1 is the Townsend parameter.

The strong depressed of a_1 (with respect ot the value 0.015 in 2D boundary layer) as well as the continuous change of γ_m with z show a skewing in the mean of the turbulent boundary layer resulting from the shear induced by rotation. Moreover, the low value of a_1 indicate that turbulence here is much less efficient than in 2D boundary layer to extract energy from the mean flow. Finally, results show that the shear stress vector is not aligned with the mean velocity gradient in both layers. As a consequence, turbulence models which rely on the assumption of an isotropic eddy viscosity should face problems because the difference $\gamma_\tau - \gamma_g$ is large.

4 Concluding remarks

In rotating cavities, the mean flow driving force results from the interaction between the rotation induced centrifugal forces and the viscosity dominated boundary layers that lead to numerical challenging investigations that might explain the limited literature. High-order DNS and LES approaches have been presented concentrating on preserving spectral accuracy. A scenario to turbulence through global secondary instability has been obtained for the first time using DNS that confirms the possibility of a direct route through absolute instability provided a low incoming noise upstream of the primary front. Our LES prediction confirms that rotation, curvature and confinement lead to a very anisotropic and inhomogeneous turbulence. Such results should encourage the LES community to increase its effort not only on the SGS modeling but also in the use of higher-order schemes.

Acknowledgements This work was granted access to the HPC resources of IDRIS under the allocation 2009-0242 made by GENCI (Grand Equipement National de Calcul Intensif). The work was supported by CNRS in the frame of the DFG-CNRS program “LES of complex flows”. The author is indebted to all the following collaborators (cited by alphabetic order) for their active collaboration to this work: P. Bontoux, J.M. Chomaz, B.E. Launder, S. Poncet, E. Severac and B. Viaud.

References

1. Andersson, H.I. and Lygren, M. (2006). LES of open rotor-stator flow, *Int. J. Heat Fluid Flow*, 27, 551–557.
2. Crespo del Arco, E., Serre, E., Bontoux, P. and Launder, B.E. (2005). Stability, transition and turbulence in rotating cavities. In Advances in Fluid Mechanics (ed. M. RAHMAN), Dalhousie University Canada Series, 41:141–196. WIT press.
3. Davies, C. and Carpenter, P.W. (2003). Global behaviour corresponding to the absolute instability of the rotating-disk boundary layer. *J. Fluid Mech.*, 486:287–329.
4. Launder, B.E., Poncet, S. and Serre, E. (2010). Transition and turbulence in rotor-stator flows, *Ann. Rev. Fluid. Mech.*, 42:229–248.
5. Lingwood, R.J. (1997). Absolute instability of the Ekman layer and related rotating flows. *J. Fluid Mech.*, 331:405–428.
6. Littell, H.S. and Eaton, J.K. (1994). Turbulence characteristics of the boundary layer on a rotating disk. *J. Fluid Mech.*, 266:175–207.
7. Lygren, M. and Andersson, H. (2001). Turbulent flow between a rotating and a stationary disk, *J. Fluid Mech.*, 426, 297–326.
8. Owen, J.M. and Rogers, R.H. (1995). Heat transfer in rotating-disk system. Wiley.
9. Pier, B. (2003). Finite amplitude crossflow vortices, secondary instability and transition in the rotating-disk boundary layer. *J. Fluid Mech.*, 487:315–343.
10. Serre, E., Crespo del Arco, E. and Bontoux, P. (2001). Annular and spiral patterns between a rotating and a stationary disk, *J. Fluid Mech.*, 434,65–100.
11. Séverac, E., Poncet, S., Serre, E. and Chauve, M.P. (2007). Large eddy simulation and measurements of turbulent enclosed rotor-stator flows. *Phys. Fluids*, 19:085113.
12. Séverac, E. and Serre, E. (2007). A spectral vanishing viscosity LES model for the simulation of turbulent flows within rotating cavities. *J. Comp. Phys.*, 226(2):1234–1255.
13. Tadmor, E. (1989). Convergence of spectral methods for nonlinear conservation laws. *SIAM J. Numer. Anal.*, 26(1), 30.
14. Viaud, B., Serre, E. and Chomaz, J.M. (2008). Elephant mode sitting on a rotating disk in an annulus. *J. Fluid Mech.*, 598:451–464.
15. Wu, X. and Squires, K.D. (2000). Prediction and investigation of the turbulent flow over a rotating disk. *J. Fluid Mech.*, 418:231–264.